Short Communication

Preparation of Magnetic Resonance Contrast Agent Gadolinium-Containing Organic Nanoparticles and Their Electrochemical Behavior Investigation

Yongkun Kang[1] and Yanjuan Zhao[2,]*

[1] Department of Radiology, The Second Hospital of Dalian Medical University, 467 Zhongshan Road, Shahekou District, Dalian 116023, Liaoning Province, China
[2] Department of Radiology, General Hospital of Northern Theater Command, 83 Wenhua Road, Shenhe District, Shenyang 110000, Liaoning Province, China.
[*]E-mail: zhao_northern@163.com

A gadolinium-based contrast agent belongs to the group of magnetic resonance imaging contrast agents commonly used in clinical illness diagnosis and research. However, the relaxation efficiency of gadolinium-based contrast agents is low, indicating that their contrast ability, selectivity, and biocompatibility could all be improved upon. Therefore, a new prospect in the field of gadolinium-based contrast agent research is the preparation of multifunctional contrast agents. This study comprises the design, synthesis and evaluation of a novel magnetic resonance contrast agent based on organic gadolinium nanoparticles (Gd-NPs). We effectively produced Gd-NPs with particle sizes ranging from 8 to 23 nm using a condensation reaction process of 1, 2-aminothiol and a cyanide group. The longitudinal relaxation of Gd-NPs employed as magnetic resonance contrast agents was steadily reduced over time. Simultaneously, transverse relaxation was first increased and then progressively decreased, at a rate proportional to the size of Gd-NPs. The electrochemical behavior of Gd-NPs was investigated using cyclic voltammetry and electrochemical impedance spectroscopy. XRD, FTIR, and Raman were used to identify and characterize the electrodeposited products.

1. INTRODUCTION

Magnetic resonance imaging (MRI) is a diagnostic technique common in clinical imaging. It offers several key advantages: it is non-invasive, it has great soft tissue resolution, and it does not emit ionizing radiation. As a result, MRI is widely employed in the disciplines of biological research and medical imaging [1,2]. The use of an MRI contrast agent is frequently required in clinical medical

diagnostics to produce a stronger signal contrast. 40–50% of today's MRI experiments use MRI contrast agents to improve the imaging contrast [3–5]. The contrast agents currently both in use and in development in clinics can be categorized into T1 and T2 contrast agents, based on their mechanism of action. T1 contrast agent research focuses on gadolinium organic compounds, whereas T2 contrast agent research focuses on iron compounds [6,7]. For clinical usage, a magnetic resonance contrast agent must satisfy the following requirements: (1) good water solubility and sufficient stability; (2) specific targetability; (3) low toxicity to biological samples; and (4) appropriate circulation time *in vivo*, to ensure that the contrast agent can not only reach the target region quickly, but can also be easily discharged from the body.

Today, MRI contrast agents in clinical usage are all small-molecule contrast agents, with a relaxation efficiency of 3.5–5.5 mM/s and no targeting capability [8–10]. However, the insertion of hydrophobic groups into ligand molecules can greatly improve the targeting capability of MRI contrast agents to overcome this disadvantage [11]. Incorporating hydrophobic groups such as phenyl into ligand molecules, for example, can dramatically increase the compound's hydrophobicity, lipophilicity, and liver targeting. Porphyrins have a strong affinity for tumor tissue, therefore binding them into ligand molecules can help enhance the contrast agent targeting capability [12].

Both transition metals and lanthanide metals can theoretically be utilized as magnetic resonance contrast agents; however, Gd (III) chelates have so far been the most commonly used [13–15]. The outermost layer of Gd (III) has seven unpaired electrons, allowing for very powerful MRI. Combining free Gd (III) with ligands can lessen its toxicity to biological tissues. Despite their widespread use, gadolinium-containing chelate contrast agents have the following drawbacks: non-specificity, limited catalytic efficiency, and short circulation time *in vivo* [16,17]. Gadolinium accumulation in the brain, as well as nephrogenic systemic fibrosis, may occur with high dosages or recurrent use. In recent years, many researchers have inserted gadolinium contrast agents into nanoparticles [18]. Leung et al. [19] recently described a new type of contrast agent that uses DO3A as its skeleton, to which it adds a phenyl group. As a result, the relaxation efficiency of the contrast agent modified with the phenyl group is higher than that of Gd-DOTA without modification. The relaxation efficiency (R1) of Gd-L1, Gd-L2 and Gd-L3 was 4.74, 4.77 and 4.95 mM/s (400 MHz), respectively, while R1 of Gd-DOTA was 3.66 mM/s (400 MHz). Unlike Gd-DOTA, Gd-L1, Gd-L2 and Gd-L3 have low toxicity and can target tumors, the liver and kidneys.

A new Gd-NP is presented in this work. When compared to gadolinium-containing small molecule precursors, these nanoparticles featured faster longitudinal relaxation rates at the same Gd^{3+} concentration. Gd-NPs of various particle sizes can be utilized as T1 or T2 contrast agents, as the nanoparticle size impacts the relaxation rate. This study also investigated the electrochemical behavior of Gd-NPs using cyclic voltammetry (CV) and electrochemical impedance spectroscopy (EIS). Finally, the electrodeposited layer during the CV scan was also examined in this study.

2. EXPERIMENTAL

Cys (SEt) -Lys [DOTA (Gd)] -CBT was purchased from Sahn Chemical Technology (Shanghai) Co., Ltd. Tris (2-carboxyethyl) phosphine (TCEP), 1, 2-aminothiols, and cyano-benzothiazole (CBT)

were purchased from J&K Belinwell. A 100 mM solution of Cys (SEt) -LYys [DOTA (Gd)] -CBT (gadolinium precursor) and a 4 mM solution of tris (2-carboxyethyl) phosphine were prepared. Gadolinium intermediates were obtained by mixing an aqueous solution of gadolinium precursor and tris (2-carboxyethyl) phosphine with a molar ratio of 25:1 at room temperature [20]. Gadolinium intermediates were then adjusted to pH 6.0 within a Na_2CO_3 aqueous solution and stirred at room temperature to obtain dynamic organic nanoparticles, which were denoted as Gd-NPs. The Gd-NPs were prepared through oligomerization and assembly, based on the condensation reaction of biocompatible 1, 2-aminothiols and cyano-benzothiazole (CBT). The functional module of MRI imaging is Gd-DOTA chelate. Gadolinium-containing precursor molecules were reduced by tris (2-carboxyethyl) phosphine (TCEP) to form 1, 2-aminothiol groups. The Gd-oligomer with larger particle size and greater hydrophobicity was formed by a condensation reaction with a CBT cyanide group, which further self-assembled to form Gd-NPs. The self-assembled nanoparticles developed in size as a result of the hydrophobic interactions between particles. Small molecules, oligomers, and nanoparticles are all part of the system's dynamic processes. In this study, the condensation process was conducted for a duration of 1 h, 2 h and 3 h.

The morphology of the Gd-NPs was observed by transmission electron microscopy (TEM, H-700 FA). A dynamic light scatterometer (DLS, ZEN3-69) was used to measure the size of the Gd-NPs. Raman analysis was carried out at room temperature using a Raman spectroscope (Renishaw InVia, UK) with a 514 nm laser light. The electrical properties of the conductor were measured using a surface resistivity meter (RTS-9, Guangzhou Four-Point Probes Technology Co. Ltd). The electrochemical impedance spectroscopy (EIS) and cyclic voltammetry (CV) were measured with a three-electrode system: a calomel electrode as the reference electrode, a copper electrode as the counter electrode and a working electrode. First, the electrodes were polished with different metallographic sandpaper grades, and then cleaned via ultrasonic for 5 minutes in a solution of secondary water, n-hexane, and ammonia ($NH_{3x}H_2O/H_2O$: 4:1), then solutions of dilute hydrochloric acid and acetone successively, and finally dried for later use. All electrochemical measurements in the Gd-NPs dispersed 0.1 M phosphate buffer saline (PBS, pH=7.4) were recorded.

3. RESULTS AND DISCUSSION

Figure 1 illustrates the results of using TEM to examine the morphology of Gd-NPs, demonstrating that the Gd-NPs showed good dispersion, with a particle size distribution of 8–23 nm. The nanoparticles assessed by TEM in the dry state were smaller than those measured by DLS in the solution state, indicating that Gd-NPs formed in the aqueous solution had a notably swollen shape [21,22].
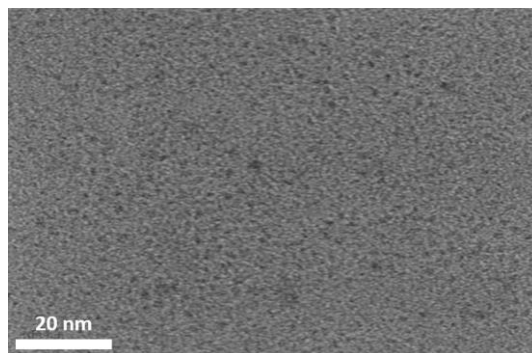
Figure 1. TEM image of prepared Gd-NPs.

Infrared spectroscopy can be used to study the interaction between different groups of molecules, as well as to analyze and determine the structure of substances and contrast agents by comparing and analyzing their position, peak strength and peak width. Figure 2 shows the FTIR spectrum of the Gd-NPs. The wave number of 3500 cm^{-1} -3000 cm^{-1} has a strong $_v$O-H vibration peak and a wider peak shape [23], which is due to the formation of a large number of hydrogen bonds in the ionic liquid such as O -- H·· O [24–27]. The wave number of 1477 cm^{-1} is the absorption peak of -CH_3 [28, 29]. Therefore, we can surmise that hydrogen bonds play a key role in the synthesis of Gd-NPs.
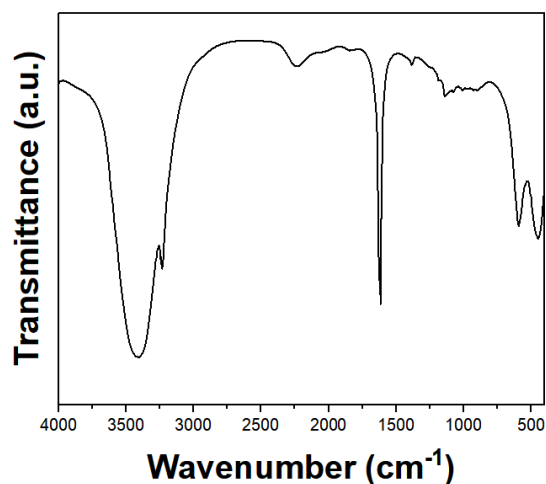
Figure 2. FTIR spectrum of prepared Gd-NPs.

Raman spectroscopy and infrared (IR) spectroscopy are complementary techniques for determining chemical structure. They each have advantages, but the Raman spectrum is better for systems containing metal components [30]. The Raman spectrum of Gd-NPs is shown in Figure 3, where it can be seen that the Gd-O Raman displacement is 595 cm^{-1} and the absorption peak is wide, which is mainly caused by the formation of hydrogen bonds in the sample. The presence of a Gd-O connection implies that the water in the contrast-like substance binds to gadolinium as coordination water [31]. These findings show that Gd-O bonds do exist in the system, which compensates for the fact that IR

spectroscopy is unable to detect Gd-O bonds. The presence of a Gd-O bond in the IR spectrum impacts the peak locations and intensities of other bonds.
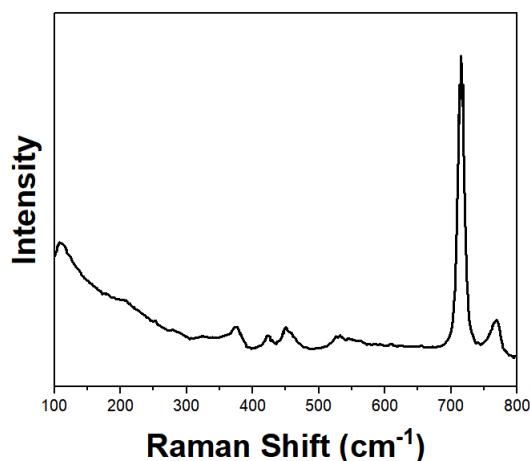
Figure 3. Raman spectrum of prepared Gd-NPs using 532 nm laser line.

CV scanning is an effective method and means by which to study electrochemistry. The CV curve can be used to identify the location of the Gd^{3+} reduction peak. Figure 4 shows the CV curve of Gd-NPs, with two reduction peaks and one oxidation peak [32]. The Gd-NPs prepared for a different length of time showed similar electrochemical behavior, whereby two reduction peaks corresponded to the reduction of dissolved oxygen and the reduction peak of Gd^{3+}. The oxidation peak can be ascribed to the OH^-, and the oxidation reaction is as follows:

$$4OH^- - 4e^- \rightarrow 2H_2O + O_2 \uparrow$$
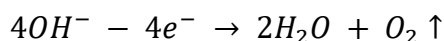
Since the system contains H_2O and Cl^-, under the condition of electricity, H_2O will preferentially discharge at the cathode and generate H_2 ($\uparrow$) and OH^-. Cl^- generates Cl_2 ($\uparrow$) at the anode and $GdCl_1(H_2O)_5^+$ accumulates near the cathode. Under the process of electrolysis, OH^- increases gradually near the cathode, and the pH value at the same location also increases [33]. Finally, Gd^{3+} may precipitate on the cathode in the form of $Gd(OH)_{3(S)}$. The electrodeposited layer was identified by XRD, and the test results are shown in Figure 5, where it can be seen that the XRD peak of the sediment is completely consistent with the standard spectrum peak of $Gd(OH)_3$, indicating that the electrodeposited layer is $Gd(OH)_3$. The likely reason for their incongruent CV curves is that the Gd-NP particle sizes are different.
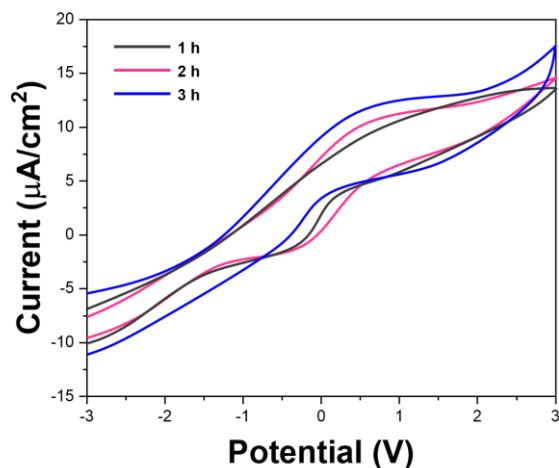
Figure 4. CV of prepared Gd-NPs recorded under 0.1 PBS (pH 7.4, scan rate 50 mV/s).
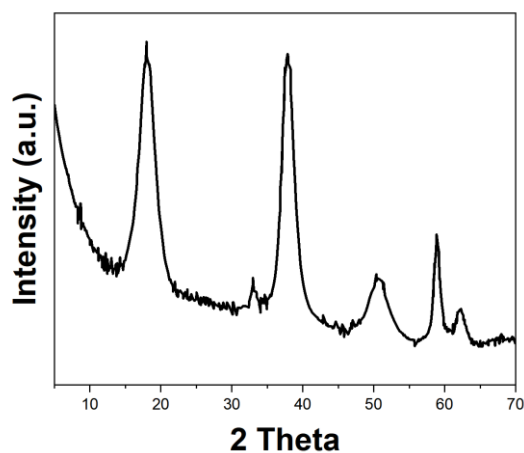
Figure 5. XRD pattern of electrodeposited layer after CV scan.

Gd-NPs with varied synthesis times were analyzed and investigated further. It can be seen from Figure 6 that the conductivity of Gd-NPs ranges from 0.140 to 14.7 mS/cm. The conductivity of the system diminishes as the synthesis time increases, owing to the formation of additional O—HO hydrogen bond networks in the system, which impedes the flow of charged particles [34]. At the same time, as the temperature rises, so too does the conductivity of Gd-NPs, since they obtain more energy and as such find it simpler to break the hydrogen link between them. Under the influence of an electric field, ion movement resistance is lowered and ion migration rate is enhanced, resulting in an increase in electrical conductivity [35].
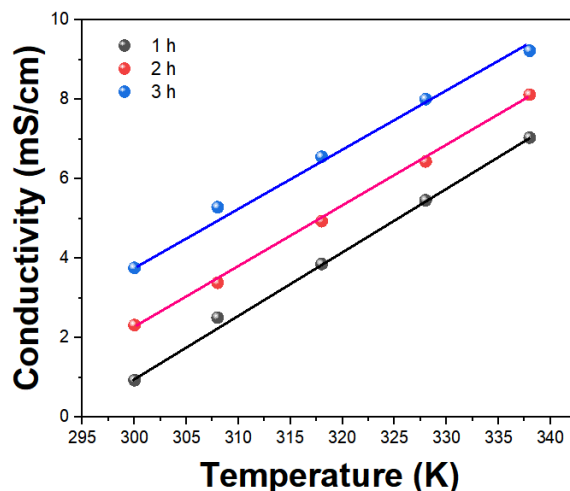
Figure 6. The conductivity of Gd-NPs as a function of preparation temperature.

EIS is a useful tool for studying the electrolyte system, as it can determine the electrolyte transfer method, while the analog circuit diagram can be used to determine the parameter values of each electrochemical element. Figure 7 depicts the EIS spectra of Gd-NPs after 1 h, 2 h, and 3 h of condensation. The impedance spectrum is represented by a semicircle in the figure, whose diameter reduces as the temperature rises. This indicates a decrease in the charge transfer resistance [36], which is conducive to the electrochemical reduction of Gd^{3+}. The solution resistance of the ionic liquid is the value of the intersection point of the curve with the Z axis in the high frequency zone. Because solution resistance is temperature-dependent, this crossing point varies depending on the length of time for synthesis [37].
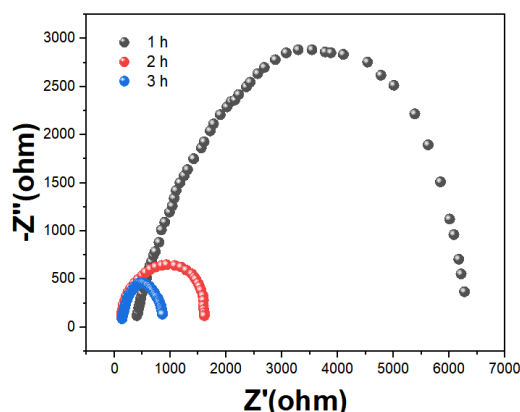
Figure 7. EIS curves of Gd-NPs prepared for 1 h, 2 h and 3 h (0.01Hz ~10^5 Hz) under 0.1 M PBS (pH 7.4).

The equivalent circuit shown in Figure 7 is used for fitting, and the parameters for this fit are listed in Table 1: R1 is the solution resistance; R2 is the polarization resistance; R3 is the charge transfer resistance; C is the double-layer capacitance; Q is the constant phase angle element caused by adsorption;

and N is the time constant, representing the relaxation process. As also seen in Table 1, solution resistance, polarization resistance, and charge transfer resistance all drop as length of time for synthesis increases, while capacitance remains relatively constant.

Table 1. EIS results obtained by fitting the experimental data

	1 h		2 h		3 h	
	value		value		value	
	Start	End	Start	End	Start	End
R1	382	383	92	92	67	67
R2	3350	3348	591	591	499	500
R3	4351	4355	531	532	38	366
C	1.21E-5	1.22E-5	5.50E-5	5.51E-5	2.81E-5	2.79E-5
Q	3.66E-5	3.65E-5	1.07E-4	1.02E-4	2.31E-5	2.30E-5
n	0.80	0.79	0.90	0.91	0.78	0.78

4. CONCLUSION

This work presents the design, synthesis, and testing of a novel magnetic resonance contrast agent based on Gd-NPs. Gd-NPs with particle sizes ranging from 8 to 23 nm were effectively produced via the condensation reaction of 1, 2-aminothiol-mercaptan with the cyanide group. The decrease in the quantityof water molecules linked to Gd^{3+} with increasing particle size can be attributed to the lowering longitudinal relaxation rate of dynamic Gd-NPs. The electrodeposited layer of the Gd-NPs process primarily consists of Gd, oxygen, and other elements. According to XRD pattern, FTIR spectrum and Raman spectrum analysis, the electrodeposited layer is $Gd(OH)_{3(S)}$, for the fundamental reason that the system contains water, and the electrolytic potential of water in the aforesaid ionic liquid system is equal to the reduction potential of Gd^{3+}. Therefore, the electrolytic potential of water is greater than that of Gd^{3+} in the electrolytic process, and the resulting product is $Gd(OH)_3$ precipitation.

References

1. K. Ghanbari, M. Roushani, E. Soheyli, R. Sahraei, *Materials Science and Engineering: C*, 102 (2019) 653.
2. T. Xiao, J. Huang, D. Wang, T. Meng, X. Yang, *Talanta*, 206 (2020) 120210.
3. Y. Zhuo, P.-X. Yuan, R. Yuan, Y.-Q. Chai, C.-L. Hong, *Biomaterials*, 30 (2009) 2284.
4. K. Tschulik, B. Haddou, D. Omanović, N.V. Rees, R.G. Compton, *Nano Research*, 6 (2013) 836.
5. Y. Wang, W. Qian, Y. Tan, S. Ding, H. Zhang, *Talanta*, 72 (2007) 1134.
6. A.A. Saei, J.E.N. Dolatabadi, P. Najafi-Marandi, A. Abhari, M. de la Guardia, *TrAC Trends in Analytical Chemistry*, 42 (2013) 216.

7. S. Hirano, N. Matsumoto, M. Morita, K. Sasaki, N. Ohmura, *Letters in Applied Microbiology*, 56 (2013) 315.
8. G. Korshin, M. Yan, *Environmental Engineering Research*, 23 (2018) 345.
9. W. Zhang, I. Soutrel, A. Amrane, F. Fourcade, F. Geneste, *Frontiers in Chemistry*, 8 (2020) 646.
10. M. Gál, F. Kielar, R. Sokolová, Š. Ramešová, V. Kolivoška, *European Journal of Inorganic Chemistry*, 2013 (2013) 3217.
11. K. Žužek Rožman, D. Pečko, S. Šturm, U. Maver, P. Nadrah, M. Bele, S. Kobe, *Materials Chemistry and Physics*, 133 (2012) 218.
12. M. Starowicz, P. Starowicz, J. Żukrowski, J. Przewoźnik, A. Lemański, C. Kapusta, J. Banaś, *Journal of Nanoparticle Research*, 13 (2011) 71676.
13. E. Bocos, N. Oturan, M.Á. Sanromán, M.A. Oturan, *Journal of Electroanalytical Chemistry*, 772 (2016) 1.
14. E. Mazario, J. Sanchez-Marcos, N. Menendez, M. Canete, A. Mayoral, S. Rivera-Fernandez, J.M. de la Fuente, P. Herrasti, *The Journal of Physical Chemistry C*, 119 (2015) 6828.
15. L. Telgmann, H. Faber, S. Jahn, D. Melles, H. Simon, M. Sperling, U. Karst, *Journal of Chromatography A*, 1240 (2012) 147.
16. M. Roostaee, I. Sheikhshoaie, *Current Biochemical Engineering*, 6 (2020) 91–102.
17. L. Cabrera, S. Gutierrez, N. Menendez, M. Morales, P. Herrasti, *Electrochimica Acta*, 53 (2008) 3436.
18. P. Vadgama, *Sensors*, 20 (2020) 3149.
19. A.H.-H. Leung, J. Jin, S. Wang, H. Lei, W.-T. Wong, *Bioconjugate Chemistry*, 25 (2014) 1112–1123.
20. B. Godin, E. Tasciotti, X. Liu, R.E. Serda, M. Ferrari, *Accounts of Chemical Research*, 44 (2011) 979.
21. S. Yadav, S.S. Nair, V. Sai, J. Satija, *Food Research International*, 119 (2019) 99.
22. Z. Garda, A. Forgács, Q.N. Do, F.K. Kálmán, S. Timári, Z. Baranyai, L. Tei, I. Tóth, Z. Kovács, G. Tircsó, *Journal of Inorganic Biochemistry*, 163 (2016) 206.
23. D. Ramimoghadam, S. Bagheri, S.B.A. Hamid, *Journal of Magnetism and Magnetic Materials*, 368 (2014) 207.
24. M. Chen, H. Yang, Z. Song, Y. Gu, Y. Zheng, J. Zhu, A. Wang, L. Fu, *Phyton-International of Experimental Botany*, 90 (2021) 1507.
25. D. Wang, D. Li, L. Fu, Y. Zheng, Y. Gu, F. Chen, S. Zhao, *Sensors*, 21 (2021) 8216.
26. L. Fu, A. Yu, G. Lai, *Chemosensors*, 9 (2021) 282.
27. H. Karimi-Maleh, C. Karaman, O. Karaman, F. Karimi, Y. Vasseghian, L. Fu, M. Baghayeri, J. Rouhi, P. Senthil Kumar, P.-L. Show, S. Rajendran, A.L. Sanati, A. Mirabi, *Journal of Nanostructure in Chemistry* (2022) in-press.
28. H. Karimi-Maleh, Y. Orooji, F. Karimi, M. Alizadeh, M. Baghayeri, J. Rouhi, S. Tajik, H. Beitollahi, S. Agarwal, V.K. Gupta, *Biosensors and Bioelectronics* (2021) 113252.
29. H. Karimi-Maleh, A. Khataee, F. Karimi, M. Baghayeri, L. Fu, J. Rouhi, C. Karaman, O. Karaman, R. Boukherroub, *Chemosphere* (2021) 132928.
30. H. Karimi-Maleh, A. Ayati, R. Davoodi, B. Tanhaei, F. Karimi, S. Malekmohammadi, Y. Orooji, L. Fu, M. Sillanpää, *Journal of Cleaner Production*, 291 (2021) 125880.
31. H. Setyawan, W. Widiyastuti, *KONA Powder and Particle Journal* (2019) 2019011.
32. T.C. Jenks, A.N. Kuda-Wedagedara, M.D. Bailey, C.L. Ward, M.J. Allen, *Inorganic Chemistry*, 59 (2020) 2613.
33. N. Ansari, Z. Payami, F. Feghhi, *Journal of Magnetism and Magnetic Materials*, 500 (2020) 166398.
34. M.A. Khayamian, S. Ansaryan, S.R. Tafti, M.S. Nikshoar, M.H. Amiri, M. Baniassadi, M. Abdolahad, *Sensors and Actuators B: Chemical*, 255 (2018) 1.
35. T.S. Rajan, T.L. Read, A. Abdalla, B.A. Patel, J.V. Macpherson, *ACS Sensors*, 5 (2020) 2858.

36. C.-J. Huang, Y.-H. Wang, P.-H. Chiu, J.-J. Lin, *Chemistry Letters*, 35 (2006) 30.
37. S. Rapino, E. Treossi, V. Palermo, M. Marcaccio, F. Paolucci, F. Zerbetto, *Chemical Communications*, 50 (2014) 13117.